Analysis of the Purcell effect in photonic and plasmonic crystals with losses

Hideo Iwase [1,3,*], Dirk Englund [1,2], and Jelena Vučković [1]

[1]*Ginzton Laboratory, Stanford University, California, 94305, USA*
[2]*Department of Electrical Engineering, Columbia University, New York, NY 10027, USA*
[3]*On leave from Canon Inc. 321-3298, Japan*
**iwase.hideo@canon.co.jp*
http://www.stanford.edu/group/nqp

Abstract: We study the spontaneous emission rate of emitter in a periodically patterned metal or dielectric membrane in the picture of a multimode field of damped Bloch states. For Bloch states in dielectric structures, the approach fully describes the Purcell effect in photonic crystal or spatially coupled cavities with losses. For a metal membrane, the Purcell factor depends on resistive loss at the resonant frequency of surface plasmon polariton (SPP). Analysis of an InP-Au-InP structure indicates that the SPP's Purcell effect can exceed a value of 50 in the ultraviolet. For a plasmonic crystal, we find a position-dependent Purcell enhancement with a mean value similar to the unpatterned membrane.

OCIS codes: (240.6680) Surface Plasmons; (130.3120) Integrated optics devices; (130.2790) Guided waves

References and links

1. E. M. Purcell, "Spontaneous emission probabilities at radio frequencies," Phys. Rev. **69**, 681 (1946).
2. M. O. Scully, and M. S. Zubairy, *Quantum Optics* (Cambridge University Press,1997), Chap. 9.
3. P. Anger, P. Bharadwaj, and L. Novotny, "Enhancement and quenching of single-molecule fluorescence," Phys. Rev. Lett. **96**(11), 113002 (2006).
4. C. Sönnichsen, T. Franzl, T. Wilk, G. von Plessen, J. Feldmann, O. Wilson, and P. Mulvaney, "Drastic reduction of plasmon damping in gold nanorods," Phys. Rev. Lett. **88**(7), 077402 (2002).
5. Y. Gong, and J. Vučković, "Design of plasmon cavities for solid-state cavity quantum electrodynamics applications," Appl. Phys. Lett. **90**(3), 033113 (2007).
6. S. A. Maier, "Plasmonic field enhancement and SERS in the effective mode volume picture," Opt. Express **14**(5), 1957–1964 (2006).
7. M. Boroditsky, R. Vrijen, T. F. Krauss, R. Coccioli, R. Bhat, and E. Yablonovitch, "Spontaneous emission extraction and Purcell enhancement from thin-film 2-D photonic crystals," J. Lightwave Technol. **17**(11), 2096–2112 (1999).
8. H. Raether, *Surface Plasmons on Smooth and Rough Surfaces and on Gratings* (Springer, Berlin, 1988).
9. K. Okamoto, I. Niki, A. Shvartser, Y. Narukawa, T. Mukai, and A. Scherer, "Surface-plasmon-enhanced light emitters based on InGaN quantum wells," Nat. Mater. **3**(9), 601–605 (2004).
10. J. Vučković, M. Loncar, and A. Scherer, "Surface plasmon enhanced light-emitting diode," IEEE J. Quantum Electron. **36**(10), 1131–1144 (2000).
11. A. Neogi, C. Lee, H. O. Everitt, T. Kuroda, A. Tackeuchi, and E. Yablonovitch, "Enhancement of spontaneous recombination rate in a quantum well by resonant surface plasmon coupling," Phys. Rev. B **66**(15), 153305 (2002).
12. I. Gontijo, M. Boroditsky, E. Yablonovitch, S. Keller, U. K. Mishra, and S. P. DenBaars, "Coupling of InGaN quantum-well photoluminescence to silver surface plasmons," Phys. Rev. B **60**(16), 11564–11567 (1999).
13. W. L. Barnes, "Electromagnetic Crystals for Surface Plasmon Polaritons and the Extraction of Light from Emissive Devices," J. Lightwave Technol. **17**(11), 2170–2182 (1999).
14. W. L. Barnes, "Fluorescence near interfaces: the role of photonic mode density," J. Mod. Opt. **45**, 661–699 (1998).
15. R. R. Chance, A. Prock, and R. Silbey, "Lifetime of an emitting molecule near partially reflecting surface," J. Chem. Phys. **60**(7), 2744–2748 (1974).
16. R. R. Chance, A. Prock, and R. Silbey, "Molecular Fluorescence and Energy Transfer near Interfaces," Adv. Chem. Phys. **37**, 1–65 (1978).
17. R. K. Lee, Y. Xu, and A. Yariv, "Modified spontaneous emission from a two-dimensional photonic bandgap crystal slab," J. Opt. Soc. Am. B **17**(8), 1438–1442 (2000).

#128920 - $15.00 USD Received 24 May 2010; revised 3 Jul 2010; accepted 4 Jul 2010; published 22 Jul 2010

18. G. Lecamp, P. Lalanne, and J. P. Hugonin, "Very large spontaneous-emission β factors in photonic-crystal waveguides," Phys. Rev. Lett. **99**(2), 023902 (2007).
19. V. S. C. Manga Tao, and S. Hughes, "Single quantum-dot Purcell factor and β factor in a photonic crystal waveguide," Phys. Rev. B **75**(20), 205437 (2007).
20. D. Sarid, "Long-range surface-plasma waves on very thin metal films," Phys. Rev. Lett. **47**(26), 1927–1930 (1981).
21. E. N. Economou, "Surface Plasmons in Thin Films," Phys. Rev. **182**(2), 539–554 (1969).
22. M. Bahriz, V. Moreau, R. Colombelli, O. Crisafulli, and O. Painter, "Design of mid-IR and THz quantum cascade laser cavities with complete TM photonic bandgap," Opt. Express **15**(10), 5948–5965 (2007).
23. J. P. Dowling, M. Scalora, M. J. Bloemer, and C. M. Bowden, "The photonic band edge laser: A new approach to gain enhancement," J. Appl. Phys. **75**(4), 1896–1899 (1994).
24. S. Nojima, "Enhancement of Optical Gain in Two-dimensional Photonic Crystals with Active Lattice Points," Jpn. J. Appl. Phys. **37**(Part 2, No. 5B), L565–L567 (1998).
25. H. A. Haus, *Waves and Fields in Optoelectronics* (Prentice Hall, New Jersey, 1984).
26. L. A. Coldren, and S. W. Corzine, *Diode Lasers and Photonic Integrated Circuits* (Wiley, New York, 1995).
27. L. D. Landau, and E. M. Lifshitz, *Electrodynamics of Continuum Media* (Pergamon, New York, 1984).
28. R. J. Glauber, and M. Lewenstein, "Quantum optics of dielectric media," Phys. Rev. A **43**(1), 467–491 (1991).
29. T. A. B. Kennedy, and E. M. Wright, "Quantization and phase-space methods for slowly varying optical fields in a dispersive nonlinear medium," Phys. Rev. A **38**(1), 212–221 (1988).
30. P. D. Drummond, and M. Hillery, "Quantum theory of dispersive electromagnetic modes," Phys. Rev. A **59**(1), 691–707 (1999).
31. Y. Jiang, and M. Liu, "Electromagnetic force in dispersive and transparent media," Phys. Rev. E Stat. Phys. Plasmas Fluids Relat. Interdiscip. Topics **58**(5), 6685–6694 (1998).
32. E. A. Hinds, "Perturbative cavity quantum electrodynamics," in *Cavity Quantum Electrodynamics*, P. R. Berman, ed. (Academic, New York, 1994).
33. H. Kuhn, "Classical aspects of energy transfer in molecular systems," J. Chem. Phys. **53**(1), 101–108 (1970).
34. J. D. Joannopoulos, R. D. Meade, and J. N. Winn, *Photonic Crystals* (Princeton University Press, New Jersey, 1995).
35. A. Chutinan, K. Ishihara, T. Asano, M. Fujita, and S. Noda, "Theoretical analysis on light-extraction efficiency of organic light-emitting diodes using FDTD and mode-expansion methods," Org. Electron. **6**(1), 3–9 (2005).
36. Y. Xu, R. K. Lee, and A. Yariv, "Quantum analysis and the classical analysis of spontaneous emission in a microcavity," Phys. Rev. A **61**(3), 033807 (2000).
37. Y. Xu, R. K. Lee, and A. Yariv, "Propagation and second-harmonic generation of electromagnetic waves in a coupled-resonator optical waveguide," J. Opt. Soc. Am. B **17**(3), 387–400 (2000).
38. J. K. S. Poon, and A. Yariv, "Active coupled-resonator optical waveguides. I. Gain enhancement and noise," J. Opt. Soc. Am. B **24**(9), 2378–2388 (2007).
39. S. C. Kitson, W. L. Barnes, and J. R. Sambles, "Full photonic band gap for surface modes in the visible," Phys. Rev. Lett. **77**(13), 2670–2673 (1996).
40. H. Iwase, D. Englund, and J. Vučković, "Spontaneous emission control in high-extraction efficiency plasmonic crystals," Opt. Express **16**(1), 426–434 (2008).
41. S. D. Liu, M. T. Cheng, Z. J. Yang, and Q. Q. Wang, "Surface plasmon propagation in a pair of metal nanowires coupled to a nanosized optical emitter," Opt. Lett. **33**(8), 851–853 (2008).

1. Introduction

The surface plasmon polariton (SPP) is a collective motion of electrons in metal that confines electromagnetic modes to the vicinity of the metal-dielectric interface. The excitonic spontaneous emission (SE) rate into a SPP cavity mode is enhanced over the vacuum decay rate Γ^0 through its spatially confined photon energy density (PED), as described by the Purcell effect [1–6]. Due to the spatial and spectral distribution of PED, the SE enhancement rate of a cavity mode, called Purcell factor F^{cav}, is proportional to the ratio of the mode's quality factor Q to its mode volume V [7]. Plasmonic cavities with large Q/V values are therefore of great interest in a wide range of applications.

Even in the absence of a cavity, metallic structures can provide a large density of optical states, and hence a large SE rate enhancement. For instance, a large density of states occurs at the metal-dielectric interface, where a field-electron resonance leads to small group velocity v^g [8] and a large enhancement in the radiative decay rate Γ [9–12]. The enhancement of Γ in the metal structure is given by $F = \Gamma/n\Gamma^0$, ignoring non-radiative recombination, where $n\Gamma^0$ is the SE rate in a bulk material with the index n. We refer to F as the Purcell enhancement factor [12]. F is the enhancement into all photonic states and is therefore distinguished from the cavity Purcell factor F^{cav} for the radiation into a cavity mode. F is a measure of the Purcell effect at a quasi-infinite metal-dielectric interface, where a number of SPP modes are involved in the SE enhancement.

#128920 - $15.00 USD Received 24 May 2010; revised 3 Jul 2010; accepted 4 Jul 2010; published 22 Jul 2010

Several approaches have been taken to analyze F for an exciton coupled to a number of propagating waves in a quasi-infinite structure [13–19]. In one approach, the 1D-confined PED is evaluated in the picture of quantum electrodynamics (QED). In analogy to the single-cavity mode volume V, the mode length L of a traveling SPP at a uniform metal-dielectric interface is considered as the normalized 1D-integral of the PED: $L = \int \partial(\omega\varepsilon)/\partial\omega \left|\mathbf{E}(z)\right|^2 dz \Big/ \max[\,\partial(\omega\varepsilon)/\partial\omega \left|\mathbf{E}(z)\right|^2\,]$ (the length is calculated in the z-direction, perpendicular to the interface) [6,12]. Evaluating L of an SPP mode with momentum $\mathbf{k}$ provides the SE rate enhancement into SPP modes with a specific $\mathbf{k}$-regime, and numerically reveals the relation between the frequency-dependence of F and the SPP's dispersion. However, in the QED picture the effect of the resistive loss on the SE into the propagating waves has not been clarified. The resistive loss strongly depends on the mode's $\mathbf{k}$ value, which determines the mode's overlap with the metal region and its group velocity [8,20–22]. The loss in the metal results in a spectral linewidth for a particular mode which has to be included in the F calculation. The total SE rate, Γ, is thus obtained by summing these SE spectra over all SPP and non-SPP modes. At the band edge of a periodic metal structure or at the SPP's resonant frequency [8,9], the SE rate into a SPP mode is particularly strongly influenced because of a high density of photonic states (slow v^g) [23,24]. Our analysis of SE in terms of $\mathbf{k}$-states with absorption-dependent linewidth represents a simple and intuitive approach for designing SPP structures to control the excitonic radiation.

In this paper, we study the Purcell enhancement factor F for the exciton coupled to SPP modes both at a uniform and periodically patterned absorptive metal-dielectric interface (or periodically patterned lossy photonic crystal), as illustrated in Figs. 1(a) and 1(b). To investigate the effect of resistive loss in a periodically patterned metal surface (plasmonic crystal), we expand the emission rates over the damped plasmonic Bloch states with different in-plane momenta $\mathbf{K}$ and quantum numbers of dispersion branches j. These states indexed by $\mathbf{K}$ and j have different quality factors $Q_{\mathbf{K},j}$. Our analysis yields the SE enhancement spectrum F^{dis} in reciprocal space, called the distributed Purcell factor, while the total spontaneous emission enhancement factor F is described as a sum of F^{dis} over all photonic states. The values of F^{dis} provide us with the Purcell enhancement ratio for the SE into a specific $\boldsymbol{k}$-mode, with resistive loss considered. Compared to the previous works, our approach reveals how the overlap of SE spectrum with the modes affects the total SE rate; this overlap has a crucial role in a slow-v^g regime. Hence, it is a useful tool to study SE enhancement in the structures, such as a patterned metal membrane or nanowire, arranged metal particles, and coupled cavities in lossy photonic crystal.

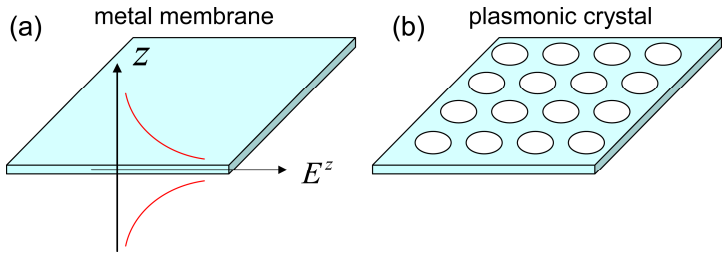

Fig. 1. (a) A metal membrane with uniform metal-dielectric interfaces and the electrical field cross-section of a SPP mode. (b) A plasmonic crystal fabricated on top of a metal membrane.

#128920 - $15.00 USD Received 24 May 2010; revised 3 Jul 2010; accepted 4 Jul 2010; published 22 Jul 2010

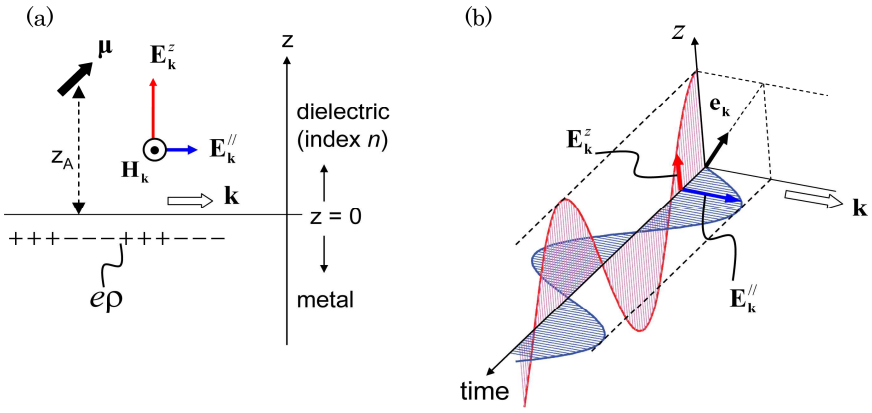

Fig. 2. (a) SPP's electromagnetic field with a momentum $\mathbf{k}$ at a uniform metal ($z \le 0$) - dielectric ($z > 0$) boundary with an area l^2. $\mathbf{E}_\mathbf{k}^z$ is an out-of-plane component of the electric field, and $\mathbf{E}_\mathbf{k}^{//}$ and $\mathbf{H}_\mathbf{k}$ are in-plane components of the electric and magnetic fields. $\mathbf{E}_\mathbf{k}^z$ and $\mathbf{E}_\mathbf{k}^{//}$ are parallel to z-direction and $\mathbf{k}$, respectively. An emitter with an electric dipole $\boldsymbol{\mu}$ lies at the distance of z_A from the metal surface (positioned at $z = 0$). (b) Time-evolution of $\mathbf{E}_\mathbf{k}^z$ and $\mathbf{E}_\mathbf{k}^{//}$ oscillating in the z-$\mathbf{k}$ plane. $\mathbf{e}_\mathbf{k}$ is a unit vector composed of the amplitudes of $\mathbf{E}_\mathbf{k}^z$ and $\mathbf{E}_\mathbf{k}^{//}$.

2. Purcell enhancement at a uniform metal-dielectric interface

Consider the geometry of Fig. 2(a) where an emitter with a frequency υ and an electric dipole $\boldsymbol{\mu}$ lies in the dielectric medium of index n, a distance z_A from the metal surface with an area l^2. An electromagnetic mode guided along the interface has an energy which decays as $e^{-\alpha x}$, where α is a decay constant and x is a distance traveled. In terms of its quality factor Q, the mode energy decays as $e^{-\omega t/Q}$, where ω is the mode frequency. By equating the last two expressions, we obtain $Q = \omega/\alpha v^g$, where v^g is the group velocity of the wavepacket [22,25,26]. The electric field of SPP mode $\mathbf{k}$ can be represented as:

$$\mathbf{E}_\mathbf{k}^{\mathrm{wp}}(\mathbf{r},t) \approx \sum\nolimits_{\Delta\mathbf{k}} \frac{A_{\Delta\mathbf{k}}}{2}\left[\mathbf{f}_{\mathbf{k}+\Delta\mathbf{k}}(\mathbf{r})e^{-i\omega_\mathbf{k}t} + \mathbf{f}_{\mathbf{k}+\Delta\mathbf{k}}^*(\mathbf{r})e^{i\omega_\mathbf{k}t}\right]e^{-\omega_\mathbf{k}t/2Q_\mathbf{k}}. \qquad (1)$$

Here, $\mathbf{f}_\mathbf{k}(\mathbf{r})$ is a normalized time-independent part of SPP's electric field with a frequency $\omega_\mathbf{k}$, and $\mathbf{f}_\mathbf{k}(\mathbf{r}) = \mathbf{u}_\mathbf{k}(z)e^{i\mathbf{k}\cdot\mathbf{x}}$, where $\mathbf{k}$ and $\mathbf{x}$ are a SPP's momentum and in-plane position vector on metal surface, respectively. In dispersive media, the electric field energy density is not $\varepsilon\mathbf{E}^2/2$ but $[\partial(\varepsilon\omega)/\partial\omega]\mathbf{E}^2/2$ [27]. Therefore, the normalization is represented as follows $\iint\partial(\varepsilon\omega)/\partial\omega\,|\mathbf{u}_\mathbf{k}|^2\,d\mathbf{r} = 1$. If $\omega_\mathbf{k}$ is smaller enough than plasma frequency ω_p with $\varepsilon = 1-\omega_p^2/\omega^2$, $\partial(\varepsilon\omega)/\partial\omega \approx|\varepsilon|$ and then $\sqrt{\partial(\varepsilon\omega)/\partial\omega}\,\mathbf{f}_\mathbf{k}(\mathbf{r}) \approx \sqrt{|\varepsilon|}\,\mathbf{f}_\mathbf{k}(\mathbf{r})$ is considered to be a normalized orthogonal field for the modes with different $\mathbf{k}$'s (it should be noted that in general $\sqrt{\varepsilon}\mathbf{E}$ of SPP is not necessarily precisely orthogonal for an arbitrary structure but approximately is, due to the frequency-dependence of ε in metal) [28]. In the microscopic picture, the field quantization in metal is required to analyze a motion of free-electron's polarization $\mathbf{P}$, and find orthogonal canonical conjugate variables, which generally relies on an effective Hamiltonian [29,30]. However, by taking the time-average of the field energy, the motion of $\mathbf{P}$ is included in an electric field energy density $[\partial(\varepsilon\omega)/\partial\omega]\mathbf{E}^2/2$ with a frequency-dependent permittivity ε [27,31]. Hence, we start with the time-averaged field energy to find canonical conjugate operators. The Hamiltonian and results of the field quantization are summarized in Appendix I.

#128920 - $15.00 USD Received 24 May 2010; revised 3 Jul 2010; accepted 4 Jul 2010; published 22 Jul 2010

Ignoring non-radiative processes, the Purcell enhancement factor F is defined as a sum of the SE rate into SPP modes, Γ^{sp}, and into non-SPP modes, $\Gamma^{non\text{-}sp}$, normalized by $n\Gamma^0$: $F \equiv (\Gamma^{sp} + \Gamma^{non-sp})/n\Gamma^0$. Here Γ^0 is a free space SE rate, $\Gamma^0 = \mu^2\upsilon^3/3\pi\varepsilon_0\hbar c^3$ [2,7,32]. By adding the decay rates for individual **k**-states (which can be obtained from the solution to the Jaynes-Cummings Hamiltonian or Fermi's golden rule, with the electric field shown in Appendix I [2,7,11,32]), we obtain the radiative decay rate Γ^{sp} into SPP modes, normalized by $n\Gamma^0$:

$$F^{sp}(\upsilon) \equiv \frac{\Gamma^{sp}}{n\Gamma^{0}} = \sum_{\mathbf{k}} \frac{2\pi}{n\Gamma^0(\upsilon)} \left|g_{\mathbf{k}}(z_A)\right|^2 D_{\mathbf{k}}(\upsilon) , \tag{2}$$

where $g_{\mathbf{k}}(z_A)$ is a coupling factor between a **k**-mode and the exciton; $g_{\mathbf{k}} = g_0\psi(z)\cos(\vartheta)$ with $g_0 = (\mu/\hbar)\sqrt{\hbar\upsilon/[(1+\Theta_{\mathbf{k}})n^2 l^2 L_{\mathbf{k}}]}$, $\psi(z) = |\mathbf{E}_{\mathbf{k}}(\mathbf{r})|/\max|\mathbf{E}_{\mathbf{k}}(\mathbf{r})|$, and $\cos(\vartheta) = \mathbf{e}_{\mathbf{k}} \cdot \mathbf{e}_{\mu}$ where $\mathbf{e}_{\mu}$ is a unit vector parallel to the excitonic dipole, and $\mathbf{e}_{\mathbf{k}} \equiv [\mathbf{u}_{\mathbf{k}}(z) + \mathbf{u}_{\mathbf{k}}^*(z)]/|\mathbf{u}_{\mathbf{k}}(z) + \mathbf{u}_{\mathbf{k}}^*(z)|$, (see Fig. 2(b) for the geometry of $\mathbf{e}_{\mathbf{k}}$) [12,28]. The mode length $L_{\mathbf{k}}$ is defined by $L_{\mathbf{k}} \equiv \int \partial(\varepsilon\omega)/\partial\omega\,|\mathbf{E}_{\mathbf{k}}(\mathbf{r})|^2\, dz \,/ \max[\partial(\varepsilon\omega)/\partial\omega\,|\mathbf{E}_{\mathbf{k}}(\mathbf{r})|^2]$, and $1/(1+\Theta_{\mathbf{k}})$ describes the ratio of the electric field energy to the total field energy ($\Theta_{\mathbf{k}} \equiv \iiint (1/\mu_0)|\nabla\times(\mathbf{f}_{\mathbf{k}}/i\omega_{\mathbf{k}})|^2\, d\mathbf{r}$, as derived in the Appendix I). The introduction of the $1/(1+\Theta_{\mathbf{k}})$ term is critical in this case, and is the result of the electromagnetic field quantization, as the energy is not equally distributed between electric and magnetic field (as described in the Appendix I). $D_{\mathbf{k}}(\upsilon)$ in Eq. (2) is the Lorentzian function describing the density of optical states (DOS):

$$D_{\mathbf{k}}(\upsilon) = \frac{1}{\pi} \frac{\omega_{\mathbf{k}}/2Q_{\mathbf{k}}}{(\omega_{\mathbf{k}} - \upsilon)^2 + (\omega_{\mathbf{k}}/2Q_{\mathbf{k}})^2} . \tag{3}$$

To analyze the Purcell enhancement of state **k**, we introduce the distributed Purcell Factor, $F^{dis}(\upsilon, \mathbf{k})$, defined as follows:

$$F^{dis}(\upsilon, \mathbf{k}) \equiv \frac{1}{\Delta k^x \Delta k^y} \frac{2\pi}{n\Gamma^0(\upsilon)} \left|g_{\mathbf{k}}(z_A)\right|^2 D_{\mathbf{k}}(\upsilon) , \tag{4}$$

where $\Delta k^x \Delta k^y \equiv (2\pi)^2/l^2$ is the reciprocal-space area of one SPP mode. If the real-space area l^2 is large enough that **k** can be considered continuous, then we can approximate Eq. (4): $F^{dis}(\upsilon, \mathbf{k}) = \partial^2 F^{sp}(\upsilon)/\partial k^x \partial k^y$. In this form, the normalized SE rate into a small reciprocal-space area $\Delta_{\mathbf{k}}$ is expressed as $F^{dis}(\upsilon, \mathbf{k})\Delta_{\mathbf{k}}$. From Eq. (4), the definition of $g_{\mathbf{k}}$, and the expression for Γ^0, $F^{dis}(\upsilon, \mathbf{k})$ becomes:

$$F^{dis}(\upsilon, \mathbf{k}) = \frac{3}{2}\frac{1}{n^3}\frac{c^3}{\upsilon^2}\frac{1}{1+\Theta_{\mathbf{k}}}\frac{h_{\mathbf{k}}(z_A)}{L_{\mathbf{k}}}\left(\mathbf{e}_{\mathbf{k}} \cdot \mathbf{e}_{\mu}\right)^2 D_{\mathbf{k}}(\upsilon) , \tag{5}$$

where $h_{\mathbf{k}}(z) = n^2 |\mathbf{E}_{\mathbf{k}}(\mathbf{r})|^2 / \max[\partial(\varepsilon\omega)/\partial\omega\,|\mathbf{E}_{\mathbf{k}}(\mathbf{r})|^2]$. $L_{\mathbf{k}}^{eff} \equiv L_{\mathbf{k}}/[h_{\mathbf{k}}(z_A)\cdot(\mathbf{e}_{\mathbf{k}} \cdot \mathbf{e}_{\mu})^2]$ is an effective mode volume for 1D-field confinement (effective mode length) [6].

Now we consider a uniform metal-dielectric interface. By integrating $F^{dis}(\upsilon, \mathbf{k})$ in polar coordinates $\mathbf{k} = (k\cos\varphi, k\sin\varphi, 0)$, we rewrite $F^{sp}(\upsilon) = \int_0^{2\pi} d\varphi \int_0^{\infty} F^{dis}(\upsilon, \mathbf{k})\, k dk = \int_0^{\infty} f(\upsilon, k) dk$, where

#128920 - $15.00 USD Received 24 May 2010; revised 3 Jul 2010; accepted 4 Jul 2010; published 22 Jul 2010

$$f(\upsilon,k)=\frac{3\pi}{n^3}\frac{c^3}{\upsilon^2}\frac{1}{1+\Theta_k}\frac{\varsigma\, h_k(z_A)}{L_k}\cdot kD_k(\upsilon)\ . \qquad (6)$$

The subscript $\mathbf{k} \to k$ indicates the values independent of φ. The factor ς results from the angular dependence of the coupling strength and averaging of $(\mathbf{e_k}\cdot\mathbf{e_\mu})^2$ over φ with $\mathbf{e_k}=(e_k^{//}\cos\varphi, e_k^{//}\sin\varphi, e_k^z)$: $\varsigma = 1/2\times(e_k^{//})^2$ when the dipole $\boldsymbol{\mu}$ is parallel to the metal surface, and $\varsigma=(e_k^z)^2$ when $\boldsymbol{\mu}$ is normal to it.

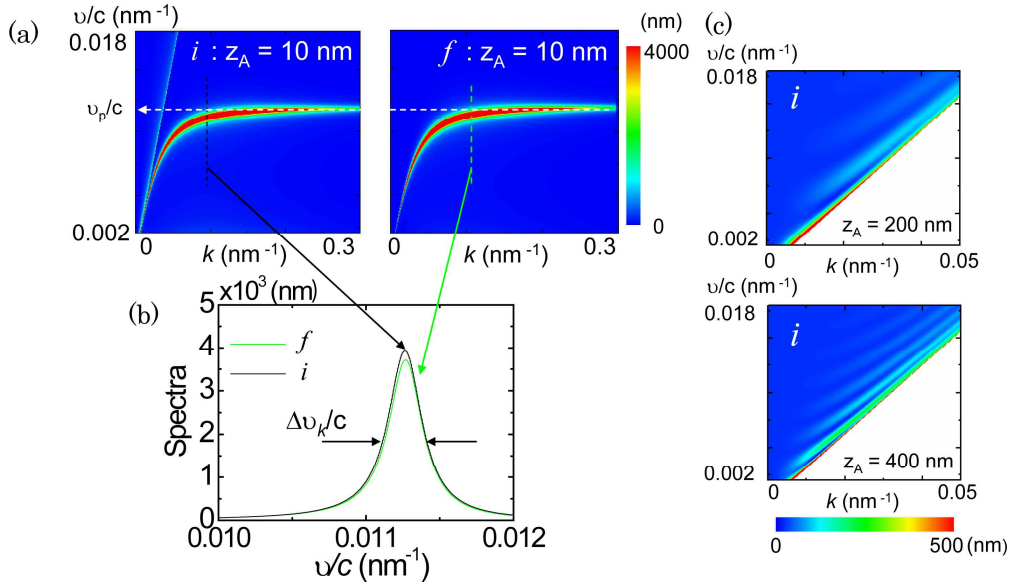

Fig. 3. (a) Distributions of the SPP spontaneous emission enhancement spectrum $i(\upsilon,k)$ by classical electrodynamics analysis (left-side panel), following References [13–16] and by quantum electrodynamics analysis, $f(\upsilon,k)$ (right-side panel). The electric dipole lies normal to the Au surface at a distance of 10 nm from it. ω_p and τ_p are set 1.21×10^{16} sec^{-1} and 1.05×10^{-14} sec, respectively. (b) Spectra of $f(\upsilon,k)$ and $i(\upsilon,k)$ at $k = 0.1$ nm^{-1} along the dashed lines in Fig. 3(a), showing an excellent match between the two analyses. The $\Delta\upsilon_k$ shows a spectral half-width. (c) Distributions of $i(\upsilon,k)$ above the light line. The distances of $\boldsymbol{\mu}$ from the Au surface are set to 200 nm and 400 nm.

In Fig. 3 we compare the distributed spontaneous emission rate enhancement $f(\upsilon,k)$ for a dipole near a uniform metal-dielectric interface obtained using the approach we presented and the classical analysis, $i(\upsilon,k)$, (from the power radiated by a classical dipole in the modified and unmodified electromagnetic environment [13–16]). For the numerical calculation, we consider an exciton close to a uniform Au/InP interface: the dipole is normal to the Au surface (for example, conduction-to-light hole band transition in a quantum well lying beneath the membrane [10,26]), the InP has index $n = 3.2$, and Au has plasma frequency $\omega_p = 1.21\times10^{16}$ sec^{-1} ($2\pi c/\omega_p = 156$ nm) and plasma life-time $\tau_p = 1.05\times10^{-14}$ sec ($\tau_p = 3.15$ μm/c). A decay constant was evaluated by the imaginary part of propagation constant k'' of SPP: $\alpha \approx 2k''$, while v_k^g and k'' are obtained by solving Maxwell's equations under the condition $\mathrm{Im}\varepsilon_p << |\,\mathrm{Re}\varepsilon_p\,|$ with $\varepsilon_p \equiv 1-\omega_p^2/(\omega^2+i\omega/\tau_p)$, as in Ref. [8]. The expressions for $i(\upsilon,k)$ for a uniform metal-dielectric boundary were also summarized by R. Chance et al. [16] and W. L. Barnes [13,14]. The resulting $i(\upsilon,k)$ and the $f(\upsilon,k)$ by Eq. (6) are plotted in Figs. 3(a) and 3(b). The area of $i(\upsilon,k)$ above the light line corresponds to SE into non-SPP modes. When the emitter is moved away from the metal surface, then $i(\upsilon,k)$ develops oscillations above the light line. This is evident in Fig. 3(c), which graphs $i(\upsilon,k)$ for emitter distances of 200 and 400 nm

#128920 - $15.00 USD Received 24 May 2010; revised 3 Jul 2010; accepted 4 Jul 2010; published 22 Jul 2010

above the metal surface. These oscillations in the emission rate are attributed to reflections from the Au surface [13–16,33]. Below the light line, which corresponds to the radiation into SPP modes, the spectral half-width $\Delta\upsilon_k$ of $i(\upsilon,k)$ is results from damp of SPP mode k with resistive loss at the dipole's position. In the spectra plotted in Figs. 3(a) and 3(b), the spectral distributions $f(\upsilon,k)$ are closely identical to the Lorentzian spectra of $i(\upsilon,k)$ in the same k-range, 0.02 $nm^{-1} < k < 0.3$ nm^{-1}.

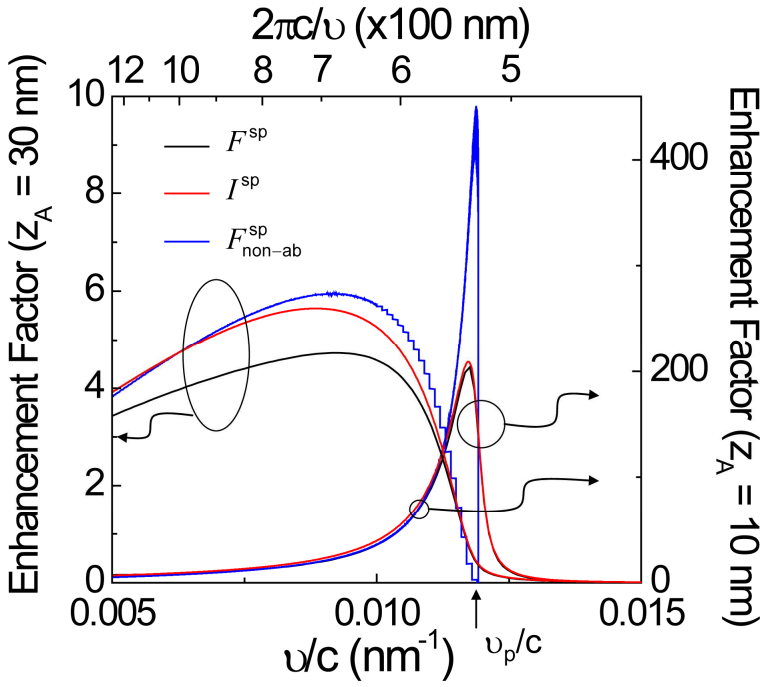

Fig. 4. Purcell enhancement factors at various frequencies from quantum analysis - F^{sp} (black lines) and classical analysis - I^{sp} (red lines) for an exciton z_A = 10 nm and 30 nm away from the Au/InP boundary, estimated by summing up $f(\upsilon,k)$ and $i(\upsilon,k)$ over $k \le 0.3$ nm^{-1}, respectively. The values of $f(\upsilon,k)$ and $i(\upsilon,k)$ for z_A = 10 nm are plotted in Fig. 3(a). Blue lines show the Purcell enhancement factor $F^{sp}_{non\text{-}ab}$ for non-absorbing media. The electric dipole lies normal to the Au surface. Non-SPP modes were ignored in the calculation of these plots.

Figure 4 compares the classical and quantum mechanically derived SE enhancement, $I^{sp}(\upsilon)$ and $F^{sp}(\upsilon)$, respectively. These were obtained by summing $i(\upsilon,k)$ and $f(\upsilon,k)$ over all SPP states, i.e., over the k-states below the light line. We additionally plot the enhancement $F^{sp}_{non-ab}(\upsilon)$ for non-absorbing media ($\tau_p \to \infty$). For the exciton lying 30 nm below the Au surface, these three estimates provide similar values. However, for a small exciton spacing of 10 nm, $F^{sp}_{non-ab}(\upsilon)$ gives a higher peak around $\upsilon_p \equiv \omega_p/(1+n^2)^{1/2}$, as absorption losses matter more for small dipole separation from the metal surface. The deviation of $F^{sp}_{non-ab}(\upsilon)$ shows that it is crucial to include the spectral spreading due to resistive loss in the slow group velocity region. On the other hand, at sufficiently low frequencies (υ/c < 0.01 nm^{-1}), the SPP dispersion approaches the light line, where the spectral spreading of $D_k(\upsilon)$ is averaged in the integration over k and results in a Purcell modification that is nearly independent of resistive loss.

#128920 - $15.00 USD Received 24 May 2010; revised 3 Jul 2010; accepted 4 Jul 2010; published 22 Jul 2010

3. Purcell enhancement in a photonic or plasmonic crystal

We will now consider 2D-plasmonic or photonic crystal structures. We take the same approach but note that the structure with a periodic permittivity $\varepsilon(\mathbf{r})$ folds the dispersion diagram into the first Brillouin zone. The normalized electric fields of SPP modes $\mathbf{f}_{\mathbf{K},j}(\mathbf{r})$ in a 2D-plasmonic crystal are represented as Bloch states [34]:

$$\mathbf{f}_{\mathbf{K},j}(\mathbf{r})e^{-i\omega t} = \mathbf{u}_{\mathbf{K},j}(\mathbf{r})e^{i\mathbf{K}\cdot\mathbf{x}}e^{-i\omega t} \ , \tag{7}$$

where $\mathbf{u}_{\mathbf{K},j}(\mathbf{r})$ with $\iiint d\mathbf{r}\left[\partial(\varepsilon\omega)/\partial\omega\right]|\mathbf{u}_{\mathbf{K},j}|^2 = 1$ is a normalized Bloch function, and $\mathbf{K}$ denotes an in-plane wave vector in the first Brillouin zone. Since the number of unit cells in the *xy*-space (with dimensions $l \times l$) is l^2/S_{cell}, where S_{cell} is the area taken by one unit cell, the mode volume $V_{\mathbf{K},j}$ for the ($\mathbf{K}$, *j*)- mode is expressed as $V_{\mathbf{K},j} = V_{\mathbf{K},j}^{\text{cell}}(l^2/S_{\text{cell}})$ where:

$$V_{\mathbf{K},j}^{\text{cell}} \equiv \iiint_{\text{unit cell}} d\mathbf{r}\partial(\varepsilon\omega)/\partial\omega\,|\mathbf{u}_{\mathbf{K},j}|^2 \Big/ \max\left[\partial(\varepsilon\omega)/\partial\omega\,|\mathbf{u}_{\mathbf{K},j}|^2\right] . \tag{8}$$

The mode's quality factor $Q_{\mathbf{K},j}$ is defined by the ratio of the energy damping rate and stored energy of the mode: $Q_{\mathbf{K},j} = \omega_{\mathbf{K},j}W_{\mathbf{K},j}\big/(\Delta_{\mathbf{K},j}^{ab} + \Delta_{\mathbf{K},j}^{\perp})$ where $W_{\mathbf{K},j}$, $\Delta_{\mathbf{K},j}^{ab}$, $\Delta_{\mathbf{K},j}^{\perp}$, and $\omega_{\mathbf{K},j}$ are the stored energy, energy absorption rate in metal, out-of-plane leakage rate, and angular frequency of the mode. Replacing $V_{\mathbf{k}}$, $Q_{\mathbf{k}}$ and $\sum_{\mathbf{k}}$ in Eqs. (2)-(6) with $V_{\mathbf{K},j}$, $Q_{\mathbf{K},j}$ and $\sum_j\sum_{\mathbf{K}}$, we obtain the Purcell enhancement factor $F^{\text{cry}}(\upsilon)$ and distributed Purcell factor $F^{\text{cry-dis}}(\upsilon,\mathbf{K},j)$ for the exciton at position $\mathbf{r}_A$ in a periodic structure:

$$F^{\text{cry}}(\upsilon) = \Delta K^x\Delta K^y\sum_j\sum_{\mathbf{K}}F^{\text{cry-dis}}(\upsilon,\ \mathbf{K},j) + \Delta K^x\Delta K^y\sum_j\sum_{\mathbf{K}}O_{\mathbf{K},j}(\upsilon) , \tag{9}$$

$$F^{\text{cry-dis}}(\upsilon,\ \mathbf{K},j) = \frac{3}{2}\frac{1}{n^3}\frac{c^3}{\upsilon^2}\frac{1}{1+\Theta_{\mathbf{K},j}}\frac{S_{\text{cell}}}{V_{\mathbf{K},j}^{\text{cell}}}h_{\mathbf{K},j}(\mathbf{r}_A)\cdot\left(\mathbf{e}_\mu\cdot\mathbf{e}_{\mathbf{K},j}\right)^2 D_{\mathbf{K},j}(\upsilon) , \tag{10}$$

where,

$$h_{\mathbf{K},j}(\mathbf{r}_A) = n^2\,|\mathbf{u}_{\mathbf{K},j}(\upsilon,\mathbf{r}_A)|^2 \,/\max\left[\partial(\varepsilon\omega)/\partial\omega\,|\mathbf{u}_{\mathbf{K},j}(\upsilon,\mathbf{r})|^2\right] . \tag{11}$$

In the above formulae, $\mathbf{e}_{\mathbf{K},j} \equiv (\mathbf{u}_{\mathbf{K},j}+\mathbf{u}_{\mathbf{K},j}^*)\big/|\mathbf{u}_{\mathbf{K},j}+\mathbf{u}_{\mathbf{K},j}^*|$, $\Theta_{\mathbf{K},j} \equiv \iiint d\mathbf{r}(1/\mu_0)\,|\nabla\times(\mathbf{f}_{\mathbf{K},j}/i\omega_{\mathbf{K},j})|^2$, and $D_{\mathbf{K},j}(\upsilon)$ is defined by Eq. (3) with $Q_{\mathbf{k}}$, $\omega_{\mathbf{k}} \to Q_{\mathbf{K},j}$, $\omega_{\mathbf{K},j}$. The second term in Eq. (9), shown by the summation of $O_{\mathbf{K},j}(\upsilon)$, represents the emission into the modes that are not bound to the metal-dielectric interface. The emission into non-SPP modes or highly leaky SPP modes can be included in the second term. We only used the properties of 2D-Bloch functions to derive Eqs. (9)-(11). Therefore, these expressions are valid for any modes described as 2D-Bloch states, no matter if the structure is a plasmonic or photonic crystal (PhC). For planar photonic crystals with negligible absorption, the Q-factor is defined by the radiation loss in the direction perpendicular to the PhC slab, i.e., $Q_{\mathbf{K},j} \to Q_{\mathbf{K},j}^{\perp} \equiv \omega_{\mathbf{K},j}W_{\mathbf{K},j}\big/\Delta_{\mathbf{K},j}^{\perp}$. In this case, $Q_{\mathbf{K},j}^{\perp}$ for the modes located under the light line approaches infinity, and the spectrum $D_{\mathbf{K},j}(\upsilon)$ is expressed by a Dirac's δ-function [35,36].

3a Purcell enhancement in a coupled photonic crystal cavity array

As the first example of the use of Eqs. (9)-(11), we will now analyze the Purcell effect for an exciton located in an array of coupled high-Q resonators embedded in photonic crystal

#128920 - $15.00 USD Received 24 May 2010; revised 3 Jul 2010; accepted 4 Jul 2010; published 22 Jul 2010

[37,38]. Figure 5(a) shows a 1D-array of resonators, described by the permittivity $\varepsilon(\mathbf{r})$. The spacing of the resonators is large enough for a small mode overlap that results in weak, nearest-neighbor coupling. The resonators themselves consist of single defects in a 2D-photonic crystal, given by $\varepsilon^0(\mathbf{r})$ as shown in Fig. 5(b), and have resonant fields $\mathbf{E}_j^0(\mathbf{r})$. The field of the array is then described as the superposition of the single-defect modes, $\mathbf{E}_{K,j}(\mathbf{r}) = A\exp(i\omega_{K,j}t)\sum_m e^{imKR}\mathbf{E}_j^0(\mathbf{r}-mR\mathbf{e}_x)$, where j denotes the mode of the single defect cavity, and $R\mathbf{e}_x$ and K are a lattice vector and a mode's momentum, respectively. The frequency of the 1D array differs from the single defect resonance Ω^j due to the coupling as follows: $\omega_{K,j} = \Omega^j[1-\Delta\alpha/2+\Delta\kappa\cos(KR)]$ where $\Delta\kappa = \int d\mathbf{r}[\varepsilon^0(\mathbf{r}-R\mathbf{e}_x)-\varepsilon(\mathbf{r}-R\mathbf{e}_x)][\mathbf{E}_j^0(\mathbf{r})\mathbf{E}_j^0(\mathbf{r}-R\mathbf{e}_x)]$ is a coupling coefficient between the neighboring defect modes and $\Delta\alpha = \int d\mathbf{r}[\varepsilon(\mathbf{r})-\varepsilon^0(\mathbf{r})][\mathbf{E}_j^0(\mathbf{r})]^2$ [37]. Assuming that the overlap of the nearby resonators is weak enough that $\int d\mathbf{r}\varepsilon^0(\mathbf{r})\mathbf{E}_j^0(\mathbf{r})\mathbf{E}_j^0(\mathbf{r}-R\mathbf{e}_x) << \int d\mathbf{r}\varepsilon^0(\mathbf{r})[\mathbf{E}_j^0(\mathbf{r})]^2$, and $h_{K,j}(\mathbf{r}_A)\cdot(\mathbf{e}_\mu\cdot\mathbf{e}_{K,j})^2 = 1$, we obtain the Purcell enhancement factor shown for the modes of the branch j:

$$F^j(\upsilon) = 2\pi\Delta K\sum_K \frac{3}{4}\frac{1}{n^3}\frac{c^3}{\upsilon^2}\frac{R}{V_{K,j}^{\text{cell}}}D_{K,j}(\upsilon), \qquad (12)$$

where $\Delta K = 2\pi/l$. To obtain Eq. (12) for PhC in dielectric media, $1/(1+\Theta_{\mathbf{k}})$ is set equal to 1/2 [28]. Equation (12) shows that the deviation of the frequencies $\omega_{\mathbf{K},j}$ from Ω^j due to the interactions causes wider spectral spreading of $F^j(\upsilon)$ than the SE spectrum of a single resonator [38]. Taking the limit of $R \to \infty$, $F^j(\upsilon)$ will approach the Purcell factor for the single defect cavity shown in Fig. 5(b). Hence, in the weak coupling condition, $F^j(\upsilon)$ can be understood as a Purcell factor of a high-Q resonator which is affected by the energy exchange to the neighboring defects.

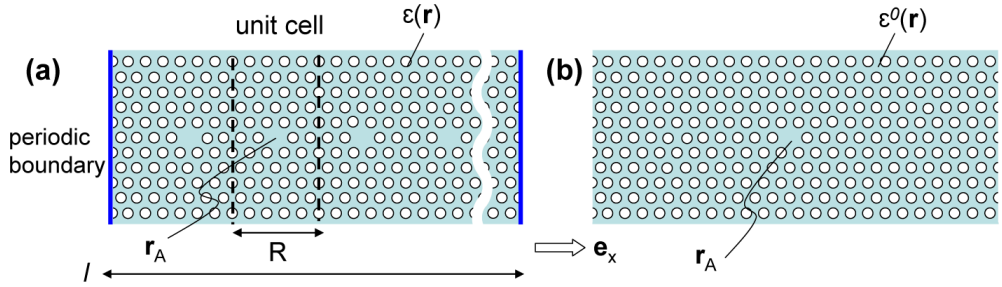

Fig. 5. (a) 1D-array of high-Q resonators, composed of defects in 2D-photonic crystal with a periodic permittivity $\varepsilon(\mathbf{r})$. The defects are aligned in x-direction with a lattice vector $R\mathbf{e}_x$. An exciton lies at the position $\mathbf{r}_A$ in a defect. (b) A single defect in a 2D-photonic crystal with a permittivity $\varepsilon^0(\mathbf{r})$.

3b Purcell enhancement in a plasmonic crystal

We also investigate the effect of periodic patterning on the Purcell effect in a gold membrane with hexagonally arranged dielectric holes, sandwiched by half-infinite InP layers, as shown in Fig. 6(a). (The Purcell enhancement in such a structure without any patterning is studied in the Appendix II). The thickness of the Au layer is 20 nm, and the periodicity of the crystal and radius of the InP holes are a = 450 nm and r/a = 0.2, respectively. We call this structure a "plasmonic crystal". For simplicity, we considered only antisymmetric SPP modes around the Γ-point. These modes are particularly interesting in plasmonic devices because of low resistive losses and vertical emission from the metal surface (The effect of resistive losses on the Purcell effect in an unpatterned InP/Au/InP structure is summarized in Appendix II).

#128920 - $15.00 USD Received 24 May 2010; revised 3 Jul 2010; accepted 4 Jul 2010; published 22 Jul 2010

Figure 6(b) shows the dispersion diagram for antisymmetric modes around the Γ -point, obtained by a Finite Difference Time Domain (FDTD) simulation. The dispersion of the antisymmetric modes in the unpatterned InP/Au/InP structure is shown in the dashed lines, which are folded into the first Brillouin zone of the hexagonal lattice [7]. The plasmonic crystal dispersion is represented by the dots, which was verified to match the dashed line in the limit of vanishing hole radii. Figure 7(a) shows the components of the electrical field belonging to the lower and upper edges of the plasmonic band gap [39]. The lower and upper bands both consist of three orthogonal modes (a monopole and two dipoles), and their field maxima are located beneath the Au layer and the dielectric holes, respectively. The electric field at the lower band (metal band) is confined out-of-plane, but the fields in the upper band (dielectric band) have large leakage losses. The Q-factors at the Γ -point are 96 for the monopole and 80 for the dipoles in the metal band, and less than 10 in the dielectric band. The Q-factors of the metal band are close to the one for an unpatterned structure: $Q_k|_{k=G} = 98$ with $G = 4\pi/\sqrt{3}a$.

In the studied structure, only SPP modes around the Γ -point are strongly affected by the periodical patterning, because of weak scattering by the holes in a thin metal membrane; the modes far from the Γ-point are not affected significantly relative to unpatterned structure. We here investigate the change of SE rate of coupling to the modes around the Γ -point, which is observable as the vertical emission from the membrane. From the field patterns shown in Fig. 7(a), we estimate the values of $V_{\mathbf{K},j}^{\text{cell}} / S_{\text{cell}}$ for the monopole and dipole components in the metal band at Γ-point to be 56 nm and 65 nm, respectively. On the other hand, for the modes belonging to the dielectric band, the values of $V_{\mathbf{K},j}^{\text{cell}} / S_{\text{cell}}$ could not be accurately evaluated because of their large leakage loss. This indicates that the coupling strength into the dielectric bands is much weaker than that into the metal band around the Γ -point. Hence, although the field components shown in Fig. 7(a) overlap with the whole surface of the membrane (both on the metal and dielectric holes), the difference of the field confinements in the metal and dielectric bands produces the position-dependence of SPP's coupling strength for the observable vertical emission [40].

To estimate the effect of the patterning on the Purcell enhancement, we compare the sum of the density of optical states in the periodic plasmonic crystal $\sum_j \sum_{\mathbf{K}} D_{\mathbf{K},j}(\upsilon)$ relative to an unpatterned structure (the structure in the limit of vanishing hole radii, studied in the Appendix II) around Γ-point ($K \le 0.0005$ nm^{-1}). We ignored dielectric bands because of their weaker coupling strengths at Γ-point. This comparison is shown in Fig. 7(b). It indicates that the change of the density of states is small around Γ-point, and thus the enhancement at the band edge is not visible because of large spectral width (induced by losses) and a small region of $v^g \approx 0$. Therefore, in the studied frequency range, the development of the low group velocity regions in the plasmonic crystal is not leading to an enhancement in the spontaneous emission rate relative to an unpatterned metal-dielectric structure. However, we should point out that patterning can certainly help in improving the light extraction from the structure, so the collected emission at the output can be larger.

It should be noted that for a structure with strong patterning induced perturbation such as holes engraved in both metal and dielectric layers, a wide band gap and a wider small-v^g region can appear in a dispersion diagram. In this case, it is required to consider all SPP modes in an interested frequency range, following the formulae in Eqs. (9) and (10).

#128920 - $15.00 USD Received 24 May 2010; revised 3 Jul 2010; accepted 4 Jul 2010; published 22 Jul 2010

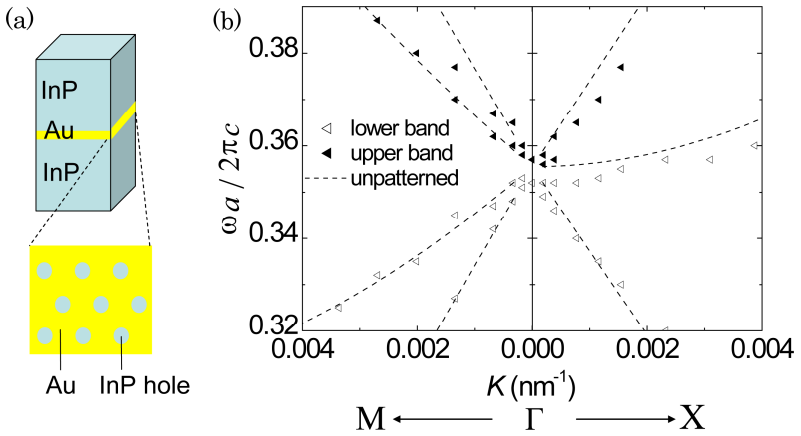

Fig. 6. (a) The plasmonic crystal consists of hexagonally arranged InP-filled holes in the Au membrane. The thickness of the Au layer is 20 nm, and the periodicity of the crystal a and radius r of the InP holes are determined by a = 450 nm and r/a = 0.2. (b) Dispersion diagrams of antisymmetric modes in the plasmonic crystal, obtained by FDTD simulation (dots). Dashed lines show the dispersion branches of the unpatterned InP/Au/InP structure.

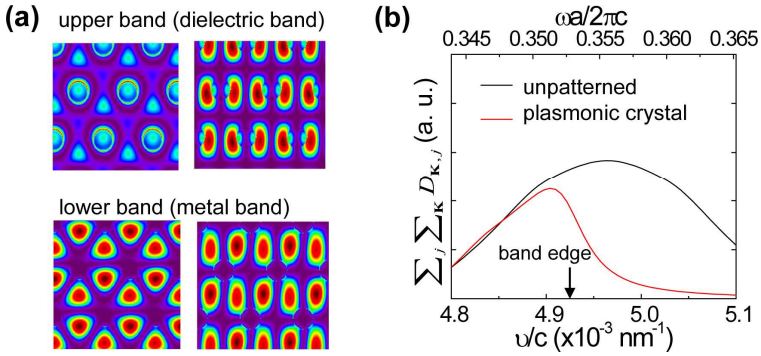

Fig. 7. (a) Field patterns on surface of Au layer in the plasmonic crystal, belonging to the upper edge (top figures) and the lower edge (bottom figures) of the plasmonic band gap shown in Fig. 6(b), obtained by FDTD simulation. The field of each band edge consists of three orthogonal modes (monopoles in the left figures and dipoles in the right figures). At the band edge, three dispersion branches overlap so close that their eigen-modes could not be separated by our FDTD simulation. (b) The sum of the density of photonic states $\sum_j \sum_{\mathbf{K}} D_{\mathbf{K},j}(\upsilon)$ for the plasmonic crystal (red line) and unpatterned structure (black line). For computation, we take the summation over the region $K \le 0.0005$ nm^{-1}, considering the degeneracy of each branch. The Q-factor for the plasmonic crystal and unpatterned structure equals 96 and 98 by FDTD simulation, respectively. In the estimation, the upper branches were ignored because of the large leakage loss.

4. Conclusion

We evaluated the full Purcell enhancement factor $F(\upsilon)$ by summing contributions to the spontaneous emission rate enhancement $f(\upsilon,\mathbf{k})$ over various points of the photonic/plasmonic band diagram $\mathbf{k}$. $F(\upsilon)$ for a uniform metal layer has large resistive loss-dependence at the SPP resonant frequency of $\upsilon_p = \omega_p/(1+n^2)^{1/2}$, where ω_p is the metal's plasma frequency. Around the frequencies where the group velocity v^g vanishes, it is essential to consider resistive loss. Otherwise, the width of the photon energy spectrum is neglected and $F(\upsilon)$ overestimated. A large Purcell enhancement in the slow-v^g regime is therefore achievable only in extremely low-resistive metal (i.e., a metal with less defect and surface-roughness at low temperature). On the other hand, the Purcell enhancement in the infrared due to the exciton-SPP coupling is

#128920 - $15.00 USD Received 24 May 2010; revised 3 Jul 2010; accepted 4 Jul 2010; published 22 Jul 2010

almost independent of resistive loss because the spectral width is greatly diminished in summing $f(\upsilon,k)$ over **k**. Hence, the approximation of non-absorbing media reliably estimates $F(\upsilon)$ in the infrared.

For 2D-periodic structures, our approach links $F(\upsilon)$ to Bloch states and $F^{\mathrm{cav}}(\upsilon)$ for a single unit cell (or single cavity inside of the cavity array). The Purcell enhancement for antisymmetric SPP in a Au membrane with a plasmonic crystal shows that the position-dependence of the Purcell enhancement depends on the leakage loss of the SPP and its field redistribution. In a hexagonal plasmonic crystal, large leakage loss of the dielectric (upper) band weakens the SPP's coupling of the emitters beneath the dielectric holes, while the emitters beneath the metal region strongly radiate into SPP. This result agrees with our experimental observation of the Purcell effect for wave-guided antisymmetric SPP modes [40]. Although the precise form of the dispersion and field patterns is required to estimate the total Purcell enhancement factor, our approach enables an analysis of the Purcell effect in plasmonic crystals with respect to SE spectra, as opposed to CED analyses relying on the total power dissipation. In this work, we focused on plasmonic crystals, but our approach is also applicable to emitters coupled to nanowires, in which traveling waves are two-dimensionally confined [41]. The theoretical platform discussed in this paper is a useful tool to fully describe the Purcell effects in photonic and plasmonic crystals, and spatially coupled cavities.

Appendix I: EM field quantization

The electromagnetic field of a mode with a particular k-vector can be described as follows [28]:

$$\mathbf{E}(\mathbf{r},t)=\frac{1}{2}\left[D\mathbf{f}_k(\mathbf{r})\eta(t)+c.c.\right] , \tag{13}$$

$$\mathbf{H}(\mathbf{r},t)=\frac{1}{2}\frac{1}{\mu_0}\left[\frac{D}{\omega_k}\nabla\times\mathbf{f}_k(\mathbf{r})\chi(t)+c.c.\right] , \tag{14}$$

and

$$\eta(t)=q(t)+ip(t) , \tag{15a}$$

$$\chi(t)=p(t)-iq(t) , \tag{15b}$$

where $q(t)\equiv\cos(\omega_k t)$ and $p(t)\equiv-\sin(\omega_k t)$ describe time-varying (oscillating) parts, μ_0 is the magnetic permeability of free space, and D is a constant. As described previously, $\mathbf{f}_k(\mathbf{r})$ is a normalized time-independent part of electric field: $\mathbf{f}_k(\mathbf{r})=\mathbf{u}_k(z)e^{i\mathbf{k}\cdot\mathbf{x}}$ with $\iiint\partial(\varepsilon\omega)/\partial\omega\,|\mathbf{u}_k|^2\,d\mathbf{r}=1$. The total energy can then be expressed as [27]:

$$W=\frac{1}{2}\iiint\left[\partial(\varepsilon\omega)/\partial\omega\mathbf{E}(\mathbf{r},t)^2+\mu_0\mathbf{H}(\mathbf{r},t)^2\right]d\mathbf{r}$$

$$=\frac{1}{4}D^2\left(p^2+q^2\right)+\frac{1}{4}D^2\Theta_k\left(p^2+q^2\right)=\frac{1}{2}D^2\frac{1+\Theta_k}{2}\left(p^2+q^2\right) , \tag{16}$$

where and $1/(1+\Theta_k)$ describes the ratio of the electric field energy to the total field energy ($\Theta_k\equiv\iiint(1/\mu_0)\,|\nabla\times(\mathbf{f}_k/i\omega_k)|^2\,d\mathbf{r}$). The choice of $D=-i\sqrt{2\omega_k/(1+\Theta_k)}$ leads to satisfying of the Hamilton's equations:

$$-\frac{\partial W}{\partial q}=-\omega_k q=\dot{p} , \tag{17a}$$

#128920 - $15.00 USD Received 24 May 2010; revised 3 Jul 2010; accepted 4 Jul 2010; published 22 Jul 2010

$$-\frac{\partial W}{\partial p}=\omega_k p=\dot{q}\ . \tag{17b}$$

Then the mode can be represented as a harmonic oscillator and the quantized Hamiltonian and electromagnetic fields are:

$$H=\hbar\omega_k\left(a^{+}a+\frac{1}{2}\right), \tag{18}$$

$$\mathbf{E}(\mathbf{r},t)=i\sqrt{\frac{\hbar\omega_k}{1+\Theta_k}}\mathbf{f}_k(\mathbf{r})a+H.C.\,, \tag{19}$$

$$\mathbf{H}(\mathbf{r},t)=\sqrt{\frac{\hbar}{(1+\Theta_k)\omega_k}}\frac{1}{\mu_0}\nabla\times\mathbf{f}_k(\mathbf{r})a+H.C.\,. \tag{20}$$

The Fig. 8 below shows the $1/(1+\Theta_k)$ and contributions of the perpendicular and parallel electric field and magnetic field components to total energy for SPP's at Au/InP interface.

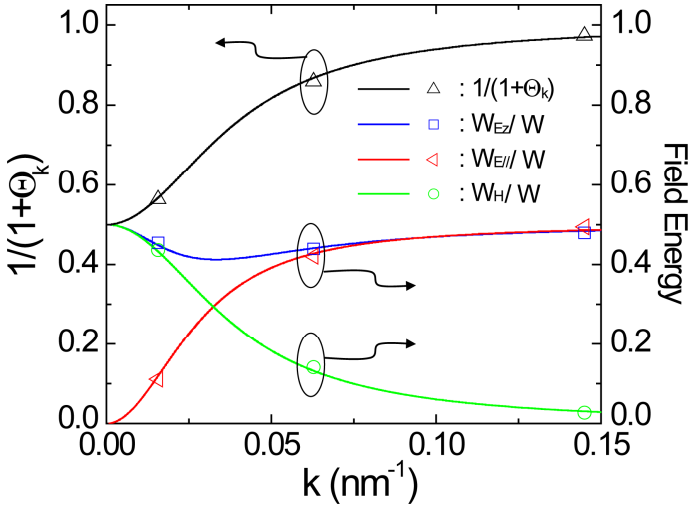

Fig. 8. Values of $1/(1+\Theta_k)$, W_{Ez}/W, $W_{E//}/W$, and W_H/W plotted for different k's for a SPP mode at Au/InP interface, where $W_{E//}\equiv\frac{1}{2}\iiint\partial(\omega\varepsilon)/\partial\omega\,|\,\mathbf{E}_k^{//}\,|^2\,d\mathbf{r}$, $W_{Ez}\equiv\frac{1}{2}\iiint\partial(\omega\varepsilon)/\partial\omega\,|\,\mathbf{E}_k^{z}\,|^2 d\mathbf{r}$, $W_H\equiv\frac{1}{2}\iiint\mu_0\,|\,\mathbf{H}_k\,|^2\,d\mathbf{r}$, and W is a k-mode's total field energy. The lines show the values estimated by analytically solving Maxwell's equations [21], and the marks by FDTD. The index and plasma frequency at Au/InP interface are set n = 3.2, and $2\pi c/\omega_p$ = 156 nm, respectively.

Appendix II: Purcell enhancement in a uniform semiconductor-metal-semiconductor structure

We consider the Purcell enhancement in a semiconductor-metal-semiconductor structure following the classical analyses by R. Chance et al. [16] and W. L. Barnes [13,14].

The structure is shown in Fig. 9(a) and consists of a 10 nm thick Au membrane sandwiched by InP. In this structure, the dispersion diagram of SPP is split into symmetric and antisymmetric modes [8,20,21], whose electric fields parallel to Au surface are shown in the bottom of Fig. 9(a). The antisymmetric modes have less resistive loss than symmetric modes

#128920 - $15.00 USD Received 24 May 2010; revised 3 Jul 2010; accepted 4 Jul 2010; published 22 Jul 2010

because of their smaller overlap with a metal membrane. The dissipation spectrum $i^{layer}(\upsilon,k)$ for this structure has been derived by R. Chance et al. [16], and is graphed in Figures 9(b) and 9(c) for an exciton 10 nm from Au surface. In these plots, the $i^{layer}(\upsilon,k)$ below the light line is expressed as the sum of two Lorentzian spectra, which correspond to SE into symmetric and antisymmetric modes, respectively: $i^{layer}(\upsilon,k) = i^{sym}(\upsilon,k)+i^{anti}(\upsilon,k)$. Figure 10(a) shows the Q-factor $\upsilon_k^0/\Delta\upsilon_k$ for the symmetric and antisymmetric modes at room temperature (RT) ($\tau_p = 1.05\times10^{-14}$ sec) and 77 K ($\tau_p = 3.27\times10^{-14}$ sec), estimated by fitting $i^{layer}(\upsilon,k)$ with Lorentzian spectra. The values of $\upsilon/2k''v_k^g$ for the antisymmetric modes, analytically evaluated as in Reference [8], are also plotted in Fig. 10(a) (blue circles) and in close agreement with the corresponding $\upsilon_k^0/\Delta\upsilon_k$. As expected, the values of $\upsilon_k^0/\Delta\upsilon_k$ for the antisymmetric modes are larger than those for symmetric modes, due to less absorption in the Au membrane. Fig. 10(b) shows the sums of the dissipation spectra, $I^{sym}(\upsilon)\equiv\sum_k i^{sym}(\upsilon,k)$ and $I^{anti}(\upsilon)\equiv\sum_k i^{anti}(\upsilon,k)$. According to the comparison between QED and CED analyses, which are made in Section 2 for a single metal-dielectric boundary, $I^{sym}(\upsilon)$ and $I^{anti}(\upsilon)$ are considered to be the enhanced SE rate into symmetric and antisymmetric modes, normalized by $n\Gamma^0$, respectively. Comparing $I^{anti}(\upsilon)$ shown in Fig. 10(b) with $i^{anti}(\upsilon,k)$ shown in Fig. 9(b), it is evident that the small-v^g regime of the antisymmetric mode's dispersion diagram results in a peak in $I^{anti}(\upsilon)$ at $\upsilon=\upsilon_{v=0}$, where a large number of $i^{anti}(\upsilon,k)$ overlap at the same frequency. As for a single metal-dielectric boundary, a high susceptibility to resistive loss is observed in the slow group velocity region at $\upsilon=\upsilon_{v=0}$.

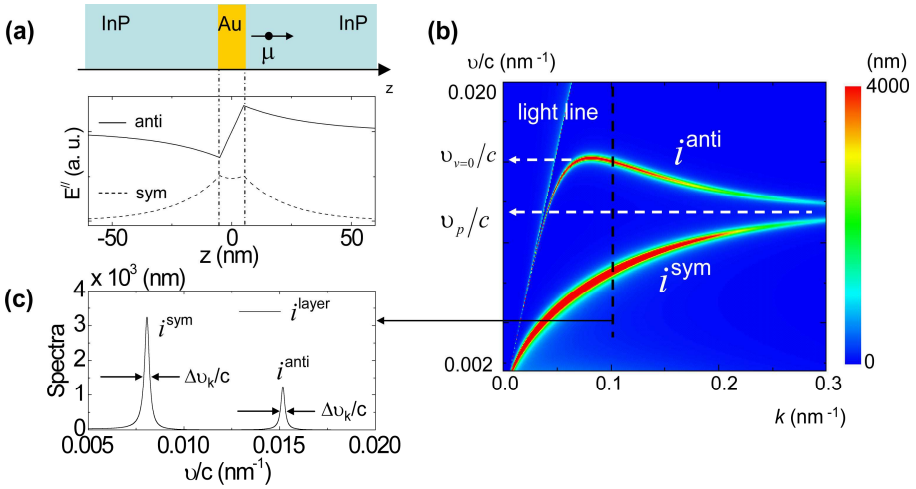

Fig. 9. (a) An InP/Au/InP structure with an electric dipole lying on the dielectric side (top), and electric field components parallel to the Au surface of an antisymmetric and symmetric modes (bottom). The Au membrane is 10 nm thick. The electric dipole lies normal to the Au surface at a distance of 10 nm apart from it. (b) The distribution of $i^{layer}(\upsilon,k)$ estimated for the structure shown in Fig. 9(a). The $\upsilon_{v=0}$ is a frequency with $v^g=0$ for the antisymmetric modes, and $\upsilon_p\equiv\omega_p/(1+n^2)^{1/2}$. (c) Dissipation spectrum $i^{layer}(\upsilon,k)$ at $k = 0.1$ nm^{-1} along the dashed line in Fig. 9(b). The $i^{layer}(\upsilon,k)$ below the light line is expressed by the sum of two Lorentzian spectra, $i^{layer}(\upsilon,k) = i^{anti}(\upsilon,k) + i^{sym}(\upsilon,k)$, corresponding to SE into the antisymmetric and symmetric modes. The $\Delta\upsilon_k$ is a half-width of the spectrum.

#128920 - $15.00 USD Received 24 May 2010; revised 3 Jul 2010; accepted 4 Jul 2010; published 22 Jul 2010

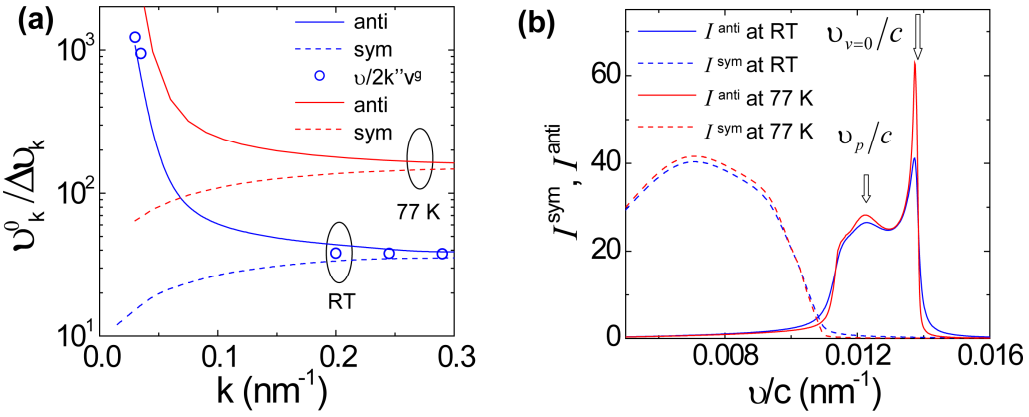

Fig. 10. (a) Quality factor $\upsilon_k^0/\Delta\upsilon_k$ of symmetric and antisymmetric modes plotted with different k's, estimated by fitting $i^{layer}(\upsilon,k)$ at RT (shown in Fig. 9(c)) and 77 K with Lorentzian spectra. The τ_p is set 1.05 × 10^{-14} sec at RT and 3.72 × 10^{-14} sec at 77 K, respectively, and ω_p = 1.21 × 10^{16} sec^{-1}. The circles show the quality factors, estimated by $\upsilon/2k''v^g$ for antisymmetric modes at RT [8]. (b) Purcell enhancements for the symmetric and anti-symmetric mode, I^{sym} and I^{anti}, at RT and 77 K, estimated by summing up i^{sym} and i^{anti} shown in Figs. 9(b) and 9(c) over $k \le 0.3$ nm^{-1}, respectively.

Acknowledgements

This work has been supported by Canon Inc. and the IFC.

#128920 - $15.00 USD Received 24 May 2010; revised 3 Jul 2010; accepted 4 Jul 2010; published 22 Jul 2010